Combustion and Flame xxx (xxxx) xxx



Contents lists available at ScienceDirect

Combustion and Flame

journal homepage: www.elsevier.com/locate/combustflame



A shock-tube study of the $N_2O+M\rightleftarrows N_2+O+M$ (M = Ar) rate constant using N_2O laser absorption near 4.6 μm

Clayton R. Mulvihill^{1,*}, Sulaiman A. Alturaifi, Eric L. Petersen

J. Mike Walker '66 Department of Mechanical Engineering, Texas A&M University, College Station, TX, United States

ARTICLE INFO

Article history: Received 29 August 2020 Revised 22 October 2020 Accepted 22 October 2020 Available online xxx

Keywords: Nitrous oxide Thermal decomposition Low-pressure limit

ABSTRACT

The low-pressure limit rate constant $k_{1,0}$ of the reaction $N_2O + M \rightleftharpoons N_2 + O + M$ was measured in shock-heated mixtures of 0.2% N_2O/Ar using 4.56-µm laser absorption of N_2O in the temperature range 1546–2476 K near 1.3 atm. Modeling the N_2O profiles with a detailed kinetic analysis, which considered non-ideal pressure variations, provided $k_{1,0}$ values that were best fit by the expression $k_{1,0} = 1.01 \times 10^{15} \exp(-30,050/T)$, with $k_{1,0}$ in cm³mol⁻¹s⁻¹ and T in K. Estimated $k_{1,0}$ uncertainties at 1546, 1821, and 2230 K were respectively 13.0%, 8.9%, and 9.0%. By combining the results of the present study with previous low-temperature data measured in flow/static reactors, the best fit over the temperature range 850–2500 K was determined to be $(k_{1,0}$ in cm³mol⁻¹s⁻¹, T in K)

$$k_{1.0} = (1.04 \pm 0.04 \times 10^{15}) \exp[(-30,098 \pm 90)/T].$$

This is the first study of $k_{1,0}$ using N₂O infrared laser absorption. Through the high signal-to-noise ratios of the experimental N₂O profiles and careful consideration of dP/dt effects, this $k_{1,0}$ determination is in excellent agreement with the large body of historical $k_{1,0}$ data but demonstrates significantly less scatter than all previous measurements.

© 2020 The Combustion Institute. Published by Elsevier Inc. All rights reserved.

1. Introduction

The spin-forbidden thermal dissociation of N₂O,

$$N_2O + M \rightleftharpoons N_2 + O(^3P) + M, \tag{R1}$$

is important to the development of unimolecular reaction theory and the generation of $O(^3P)$ atoms in chemical kinetics experiments. Consequently, the low-pressure limit rate constant, $k_{1,0}$, has been widely studied in shock tubes [1–17].

Early shock-tube studies of $k_{1.0}$ employed N₂O ultraviolet absorption (N₂O-UVA) [1,2] and infrared emission (N₂O-IRE) [2–4] to infer $k_{1.0}$. With the increasing prevalence of atomic resonance absorption spectroscopy (ARAS) in the 1960s and 1970s, O-atom ARAS (O-ARAS) was soon used to measure $k_{1.0}$ [5]. While some early $k_{1.0}$ studies employed other methods (e.g., mass spectrometry [6], gas chromatography [7], and laser schlieren densitometry [8]), these methods were ultimately eschewed in favor of N₂O-

UVA, N_2O -IRE, and O-ARAS in recent $k_{1,0}$ studies [9–17]. Several such studies are summarized in Table 1.

The previous shock-tube studies of $k_{1,0}$ are subject to multiple problems. First, signal-to-noise ratios (SNRs) were as low as ~10 for N₂O-UVA (Fig. 1c of [13]), ~12 for N₂O-IRE (Fig. 3 of [2]), and ~7 for O-ARAS (Fig. 3 of [12]). Many studies did not provide sample data with which to estimate the SNR, but overall scatter in the $k_{1,0}$ data (see the σ column in Table 1, assembled by the present authors using available literature data) is likely partially due to low SNR. Second, the kinetic analyses employed were often analytic rather than numeric. For example, some studies used the quasi-steady state (QSS) assumption for [O] (see pg. 374 of Hanson and Salimian [18]), which underestimates $k_{1,0}$ and likely explains the systematically lower $k_{1,0}$ data of Jost et al. [1], Olschewski et al. [3], and Fujii et al. [11] (Sulzmann et al. [10] also made the QSS assumption, but the large scatter in their data obscures any systematic uncertainty). Third, some studies used high N2O concentrations (~3%). Such high concentrations can lead to significant changes in temperature (~45 K after 2 ms for 2.5% N₂O in balance Ar initially at 1700 K and 1 atm) that can confound kinetic interpretations. Fourth, N2O-UVA and O-ARAS are subject to interfering absorption, which can be partially corrected for but invariably introduces uncertainty to the measurement. The N₂O-UVA studies

https://doi.org/10.1016/j.combustflame.2020.10.040

0010-2180/ $\ \odot$ 2020 The Combustion Institute. Published by Elsevier Inc. All rights reserved.

^{*} Corresponding author.

E-mail address: mulvihcr@anl.gov (C.R. Mulvihill).

 $^{^{\,1}}$ Present address: Chemical Sciences and Engineering, Argonne National Laboratory, Lemont, IL, United States.

Combustion and Flame xxx (xxxx) xxx

Table 1 Selected shock-tube studies of $k_{1,0}$ with M = Ar.

Author	Year	T ₅ range (K) ^a	P ₅ range (atm) ^a	N ₂ O mole fraction ^b	Diagnostic	Kinetic analysis method ^c	# of points	$\sigma(\%)^{\mathrm{d}}$	Ref.
Jost et al.	1964	1500-2500	2-20e	0.5-3%	N ₂ O-UVA (230 nm) ^f	$k_1 = k_{app}/2^g$	56	25.4	[1]
Olschewski et al.	1966	1500-2550	0.8-12.3h	0.02-1%	N_2O -IRE (4.5 μ m)	$k_1 = k_{app}/2$	69 ⁱ	15.8	[3]
Monat et al.	1977	1800-3350	~0.4	1-2%	N_2O -IRE $(4.5 \mu m)^j$	Numerical (9)	5	14.1	[4]
Zaslonko et al.	1980	1800-2400	2-15 ^k	2.5%	N ₂ O-UVA (240 nm) ¹	Numerical (3)	4	16.1 ^m	[9]
Sulzmann et al.	1980	1700-2550	1.7-4.6	2%	N_2O -IRE $(4.5 \mu m)^n$	$k_1 = k_{app}/2^{\circ}$	10	38.2	[10]
Fujii et al.	1986	1550-2000	~2	1%	N_2O -IRE (4.5 μ m)	$k_1 = k_{app}/2^p$	8	8.6	[11]
Fujii et al.	1989	1600-2400	~1	0.01%	O-ARAS (130 nm)	Initial slope ^q	20	16.3	[12]
Zuev and	1991	1800-2250	$2-20^{r}$	3%	N ₂ O-IRE (2.9, 4.5 μm),	Numerical (10) ^t	26	8.9 ^u	[13]
Starikovskii					N ₂ O-UVA (250 nm) ^s				
Michael and Lim	1992	1550-2500	0.7-1.1 ^v	~2 ppm	O-ARAS (130 nm)	Initial slope	36	34.2	[14]
Röhrig et al.	1996	1700-3100	0.3-6.5	0.05%, 0.5%	N_2O -IRE (4.5 μ m)	Numerical (9)	11	11.6	[15]
Ross et al.	1997	1200-2400	<1	0.0001-0.2%	O-ARAS (130 nm)	Initial slope and	131	32.5	[16]
						first order ^w			
Javoy et al.	2009	1500-2500	0.6 - 3.4	3-50 ppm	O-ARAS (130 nm)	Numerical (3)	27	20.6	[17]
This study	2020	1550-2500	1.1-1.4	0.2%	N ₂ O-IRA (4.562 μm)	Numerical (26)	15	3.1	-

- a Some works also include measurements of the high-pressure limit rate constant, $k_{1,\infty}$. The T_5 and P_5 ranges here correspond only to measurements of $k_{1,0}$.
- $^{\rm b}$ The balance in all mixtures is Ar since only datapoints from mixtures of N_2O and Ar are considered.
- ^c The number in parentheses represents the number of reactions included in the detailed mechanism.
- $^{
 m d}$ σ is defined as the standard deviation of the percent difference between the datapoints and the best-fit Arrhenius expression.
- ^e Found no pressure dependence of k_1 up to 20 atm. This finding conflicts with the later findings of [13].
- f Also measured NO UV absorption (226 nm). The NO profiles were not used for any kinetic inferences.
- ^g The apparent rate of N₂O disappearance is $k_{app} = -1/([N_2O][M])(d[N_2O]/dt)$. The factor of 2 in the expression $k_1 = k_{app}/2$ arises from the QSS assumption for [O] (see pg. 374 of [18]).
- ^h P_5 for the whole study ranged from 0.8 to 300 atm. The P_5 range for the $k_{1,0}$ measurements was not explicitly stated. However, the study of $k_{1,0}$ was performed at [M] < 6×10^{-5} mol/cm³. Assuming T_5 was 2500 K at this concentration, P_5 was thus 12.3 atm or less for the $k_{1,0}$ experiments.
- i The 0.02% N_2O data are included in the 69 total datapoints but are excluded from the calculation of σ due to inconsistencies in this dataset.
- ^j Also measured NO IR emission (5.3 μ m). Used the NO profiles to infer the ratio k_3/k_1 (see Section 3 for definition of R3).
- ^k Estimated using the stated range of [M] $(1-10 \times 10^{-5} \text{ mol/cm}^3)$ with the known T_5 range.
- ¹ Also measured NO UV absorption (214 nm). The NO profiles were not used for any kinetic inferences.
- $^{\mathrm{m}}$ The short-dashed line in their Fig. 2 was used to calculate $\sigma.$
- ⁿ Also measured NO UV absorption (226 nm). Used the NO profiles to infer $k_2 + k_3$ and the ratio k_2/k_3 (see Section 3 for definition of R2 and R3).
- ^o An initial slope method for $[N_2O]$ was also used to extract $k_{1,0}$ for some of the colder experiments.
- ^p Also simulated their results with a 3-reaction mechanism, but this mechanism was not used to extract $k_{1,0}$.
- ^q The initial slope method using [O] is $k_1 = \Delta[O]/(\Delta t[N_2O]_0[M])$, where Δt can be arbitrarily chosen and is typically taken near the beginning of the experiment.
- It is unclear at what P_5 the $k_{1,0}$ measurements were performed since $k_{1,\infty}$ was also measured in this work.
- ⁵ Also measured NO₂ visible absorption (434 nm) and NO-O recombination emission (500 nm). Used these diagnostics to infer $k_{1,\infty}$.
- ^t It is unclear whether the 10-reaction mechanism was used to simulate the actual experimental profiles or merely the extracted k_{app} values.
- ^u Since the data reported in their Fig. 2 were k_{app} values, a least-squares fit to these k_{app} data was used to calculate σ .
- ^v Estimated using the stated value of [M] $(5.5 \times 10^{-6} \text{ mol/cm}^3)$ with the known T_5 range.
- $^{\rm w}$ Initial slope analysis performed for T_5 < 1900 K. First-order analysis performed for T_5 > 1900 K.

in Table 1 employed wavelengths near 240 nm to access unresolved low-lying electronic states of N₂O [19]; these wavelengths are subject to interference from the γ bands $(A^2 \Sigma^+ \leftarrow X^2 \Pi)$ of NO [20]. The O-ARAS studies in Table 1 employed the strong triplet lines (${}^{3}S_{1}^{0} \leftarrow {}^{3}P_{2,1,0}$) of O at 130.2, 130.5, and 130.6 nm [21]; these wavelengths are subject to interference from the $D^1 \Sigma^+ \leftarrow X^2 \Sigma^+$ transition of N2O [22]. Fifth and finally, none of the studies in Table 1 save those of Fujii et al. [11,12] considered the effects of the non-ideal pressure change dP/dt, which is a shock-tube phenomenon that can have significant effects on the extraction of chemical kinetics parameters from shock-tube experiments [23]. As a result of these five complications, factor-of-three differences persist in the $k_{1.0}$ data between ~1500 and ~2500 K; see Fig. S1 in the Supplementary Material (SM). Therefore, an opportunity exists to apply a new technique to obtain improved hightemperature $k_{1,0}$ data by avoiding or improving upon these five

Since the turn of the century, the quantum cascade laser (QCL) has revolutionized access to the mid-IR (3–12 μ m) [24]. The fundamental vibrational frequencies of many organic and/or combustion-relevant species fall within the mid-IR; therefore, QCL access to this spectral region permits sensitive detection of numerous molecules [25]. Because laser-absorption schemes can be deployed with extremely high SNRs, QCLs can provide speciation measurements that are ideal for determin-

ing accurate rate constants [26], particularly at lower pressures where phenomena such as beam-steering are negligible [27].

There are no shock-tube studies of $k_{1,0}$ using N₂O infrared absorption (N₂O-IRA). Thus, this paper presents the first such measurement by employing a new, fixed-wavelength N₂O diagnostic near 4.56 μ m. The shock tube and laser diagnostic are first described, and a pair of representative experiments is analyzed in detail to illustrate the data reduction method. The $k_{1,0}$ data are then presented. Finally, discussion is given to the various details of the $k_{1,0}$ data extraction and the improvements of the present work over previous studies.

2. Experiment

2.1. Shock tube and mixing tank

Experiments were performed in a stainless-steel shock tube with a 7.62-cm diameter driver section (length: 3.0 m) and a 16.2-cm diameter driven section (length: 6.78 m). Polycarbonate diaphragms of 0.254-mm thickness were burst using He as the driver gas. Mechanical and turbomolecular pumps achieved ultimate pressures of ~ 10^{-8} atm in the driven section before each experiment. Five piezoelectric pressure transducers measured the incident shock wave velocity v_s ; the temperature T_5 and pressure P_5 behind the reflected shock wave (RSW) were calculated using

Combustion and Flame xxx (xxxx) xxx

 v_s . The sidewall pressure was monitored 1.6 cm from the driven section endwall using a piezoelectric transducer; this sensor was shielded using RTV silicone to mitigate heat transfer effects that can alter measured pressure profiles [28]. For more details on the shock tube, see Vivanco [29].

Gas-phase mixtures were prepared manometrically in a stainless-steel mixing tank using 0–0.01 and 0–17 atm pressure gauges. N₂O was supplied by Praxair at 99.5% purity; Ar was supplied by Airgas at 99.999% purity. Pressures of ~10⁻⁹ atm were achieved before mixture preparation. Mixtures were left overnight before performing experiments. All experiments used mixtures of 0.2% N₂O in balance Ar. With this low N₂O concentration, temperature decreases due to endothermicity during the timeframe of the $k_{1,0}$ determination were at most 18 K for the hottest experiment but typically less than 8 K.

To investigate potential H_2O or H contamination effects, simulations were performed with a detailed mechanism [30]. Even if the entirety of the 0.5% impurities in the N_2O bottle were H_2O , calculations with and without H_2O at the high- and low-temperature ends of this study showed no difference in terms of the modeled N_2O time histories (Praxair indicates that the majority of the impurities in N_2O is actually N_2 , which also has no effect on the model predictions). Similar calculations indicated no effect of H on the present experiments, where the amount of H was estimated as a function of T_5 using the model of Urzay et al. [31].

2.2. N₂O laser absorption diagnostic

Tunable laser light was generated to probe the P(33e) transition within the $00^{\circ}01\leftarrow00^{\circ}0$ band of N₂O. At the conditions of this study, this transition blends with the weaker P(19e) and P(19f) transitions in the $01^{1}1\leftarrow01^{1}0$ band [32]; therefore, the laser was tuned to 2192.474 cm⁻¹ (~4.561 µm) to access the peak of the blended spectral feature for optimum N₂O detectivity. No interfering absorption occurs at this frequency: NO possesses negligibly weak line strengths in this region [33], and N₂, O₂, and O are IR inactive.

A continuous-wave QCL (Alpes Lasers) provided narrow-linewidth ($\sim \! \! 5 \times 10^{-5} \ cm^{-1})$ light. The QCL was cooled with an internal thermoelectric cooler (TEC) and situated atop an external TEC for additional temperature stability. The QCL temperature and current were maintained at typical values of –24.5 °C and 375 mA via an Arroyo Instruments 6310-QCL controller. The absolute frequency of the laser was monitored using a Bristol 671B-MIR wavemeter with a resolution of 0.001 cm $^{-1}$.

The laser beam was split into two legs with a beamsplitter. One leg was directed to the reference intensity (I_0) detector, while the other was passed through the shock tube via two sapphire window ports located in the same plane as the sidewall pressure transducer and directed into the transmitted intensity (I_t) detector. The detectors (Teledyne Judson J10D, 200-kHz bandwidth) were liquid-N₂cooled and fitted with optical filters (I_0 : center 4500 nm, full-width 500 nm; I_t : center 4562 nm, full-width 33 nm). An experiment with the laser turned off confirmed that even at the high-temperature end of this study, the broadband emission exiting the shock tube was reduced to undetectable levels via the optical filters and other optics. Using common-mode rejection via a differential preamplifier, the signals I_0 and $I_0 - I_t$ were sampled at 1 MHz with a digital oscilloscope and post-processed with a first-order, 200-kHz-cutoff Butterworth filter (see Fig. S5).

3. Results

Representative transmission and pressure traces are shown in Fig. 1 for experiments near the low- and high-temperature ends of this study. The jumps at time zero mark the passage of the

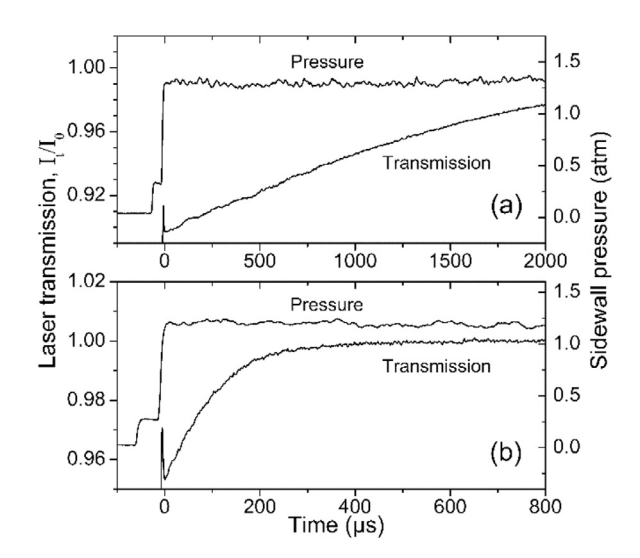


Fig. 1. Representative laser transmission and sidewall pressure traces acquired in 0.2% N_2 0/Ar at (a) 1821 K, 1.31 atm and (b) 2230 K, 1.21 atm.

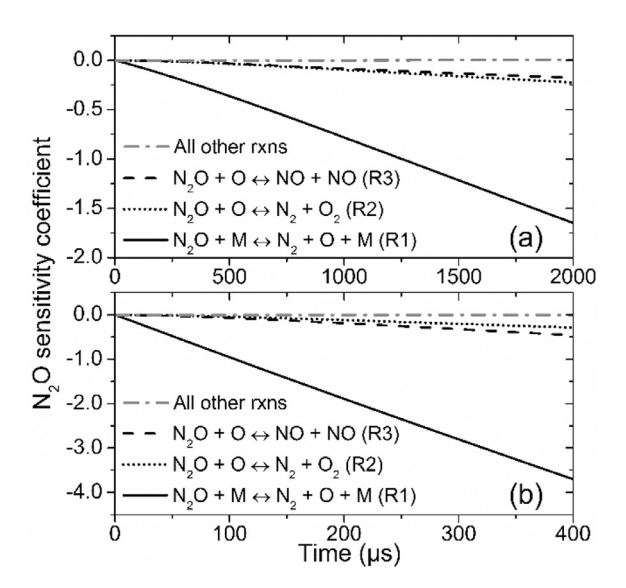


Fig. 2. N_2O sensitivity analysis at the conditions of Fig. 1 using the 26-reaction mechanism of the present study.

RSW. Following the achievement of T_5 and P_5 behind the RSW, the transmission increases as the N₂O decomposes. No signs of N₂O vibrational relaxation were observed, in agreement with indications that the 1/e vibrational relaxation time should be well below 1 μ s at these conditions [8]. Conservative estimates of the SNR are 120 and 40 for the traces in Fig. 1a and b, respectively.

To analyze the experiments, a 26-reaction, 11-species chemical kinetics mechanism for N_2O decomposition was assembled from the literature [15,30,34–41] guided by previous modeling works [30,34]. Thermodynamic data were taken from Burcat and Ruscic [42]. The mechanism is described in the SM (Table S2), and the mechanism and thermodynamic data are provided as Chemkinformat text files in the SM. Figure 2 displays the N_2O sensitivity analysis at the conditions of Fig. 1 using the 26-reaction mechanism and reveals the N_2O concentration is chiefly sensitive to R1, with only minor sensitivities to two other reactions:

$$N_2O + O(^3P) \rightleftharpoons N_2 + O_2$$
 (R2)

$$N_2O + O(^3P) \rightleftharpoons NO + NO.$$
 (R3)



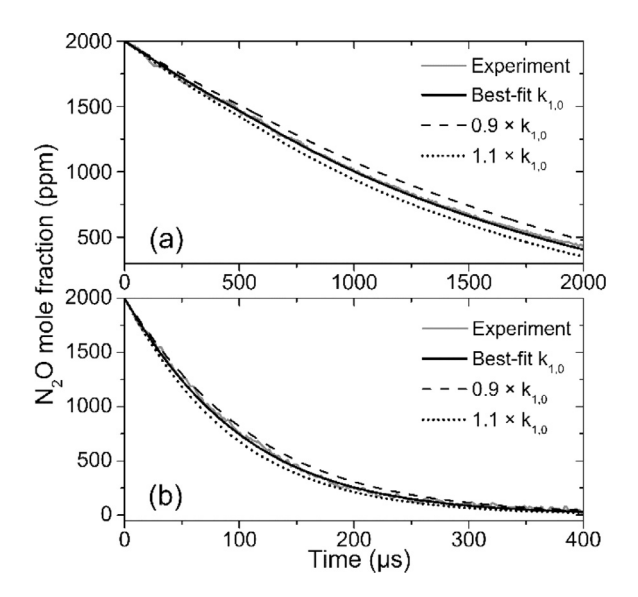


Fig. 3. N₂O time histories at the conditions of Fig. 1: (a) 1821 K, 1.31 atm and (b) 2230 K, 1.21 atm. Solid line: predictions of the 26-reaction mechanism of the present study with the best-fit $k_{1.0}$ for each individual experiment. Dotted/dashed lines: mechanism predictions with $\pm 10\%$ variations in the best-fit $k_{1.0}$.

Figure 2 shows the N_2O concentration is completely insensitive to all other reactions, making the selection of the remaining 23 reactions in the mechanism unimportant. k_2 and k_3 were taken from Meagher and Anderson [34] and are estimated to have uncertainties of 50%; see Section 4.1.

Transmission time histories were converted to N2O time histories via the Beer-Lambert law, $I_t/I_0 = \exp[-k_v(t) \cdot P(t) \cdot X_{N20}(t) \cdot L]$ Here, $k_{\nu}(t)$ is the time-varying spectral absorption coefficient, P(t)is the time-varying pressure, $X_{N2O}(t)$ is the time-varying N₂O mole fraction, and L is 16.2 cm. P(t) was the measured pressure trace. The initial $k_{\nu}(t)$, $k_{\nu,0}$, was calculated from the initial N₂O concentration (0.2%), the initial pressure (P_5), and the initial transmission behind the RSW; in this sense, the present experiments were selfcalibrating in terms of $k_{v,0}$, requiring no spectroscopic parameters for N₂O. Values of $k_{v,0}$ are plotted in Fig. S3 as a function of T_5 ; the best fit to these data is $k_{\nu,0}(T) = 86.99 \exp(-1.914 \times 10^{-3} \times T)$. At T_5 > 2000 K, rapid N₂O decomposition slightly lowers the determined $k_{\nu,0}$ by no more than 10%, but ultimately has no effect on the $k_{1,0}$ determination, as discussed later. From P(t), a time-varying temperature profile, T(t), was calculated assuming isentropic expansion/compression; this assumption has been repeatedly verified for similar conditions (e.g., [28,43,44]). T(t) was then used to calculate $k_v(t)$ using the temperature dependence of $k_{\nu,0}(T)$. With all other variables known, $X_{N2O}(t)$ was inferred. Accounting for P(t) and $k_{\nu}(t)$, rather than holding them constant, caused only minor changes in $X_{N2O}(t)$ (~ 2% or less; see Fig. S4) but was nonetheless performed for all data analyses. N2O time histories from the Fig. 1 experiments are shown in Fig. 3.

Also shown in Fig. 3 are the predictions of the 26-reaction mechanism using the best-fit $k_{1,0}$ for each experiment. The mechanism predictions were calculated using the 0-D reactor in the Chemkin-Pro-suite assuming constant internal energy and employing the volume-as-a-function-of-time (VTIM) method [45] based on the measured pressure traces; see Section 4.2. To extract the best-fit $k_{1,0}$ from each experiment, $k_{1,0}$ was adjusted until the predicted N₂O time history from the 26-reaction mechanism best matched the experimental N₂O time history using the following methodology.

Using a fixed value of E_a for all experiments, A in the Arrhenius expression $k_{1,0} = A \exp(-E_a/RT)$ was varied for each experi-

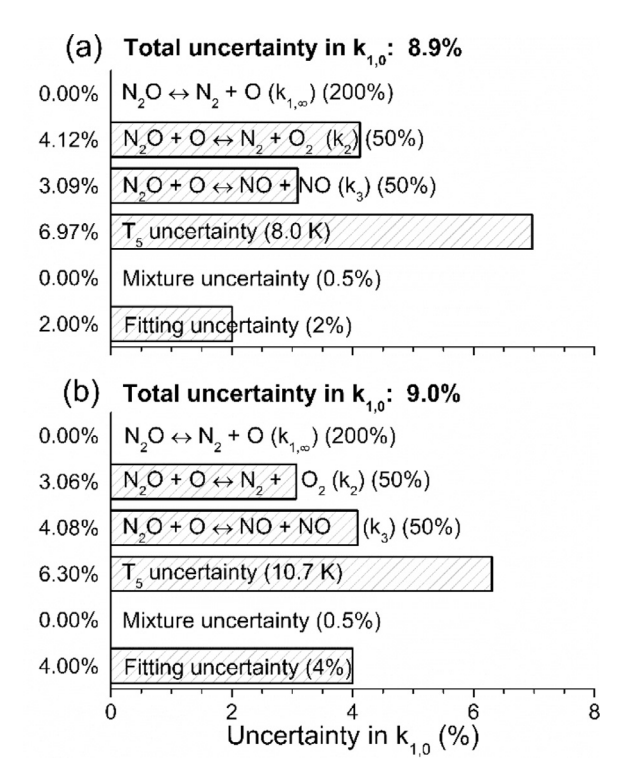


Fig. 4. $k_{1,0}$ uncertainty analyses at the conditions of Fig. 1 using the root-sum-squares method. Values in parentheses are the estimated uncertainties of each uncertainty source. $k_{1,\infty}$, k_2 , and k_3 uncertainties were taken from Baulch et al. [41]. T_5 uncertainty was assessed according to Petersen et al. [46].

ment to achieve a best fit between the modeled and experimental N_2O time histories. The experiment-specific $k_{1,0}$ value was then calculated using the best-fit A, the fixed E_a , and T_5 . Two iterations (with a different E_a for each iteration) were used to extract $k_{1,0}$ in three steps. First, Iteration 1 assumed E_a =56,644 cal/mol (according to Röhrig et al. [15]) and best-fit $k_{1,0}$ values were determined using this fixed E_a . Second, a best-fit, two-parameter Arrhenius expression was fit to the Iteration 1 $k_{1,0}$ values; this fit had E_a =59,729 cal/mol. Third, E_a = 59,729 cal/mol was fixed during Iteration 2 to determine the next set of best-fit $k_{1,0}$ values. From Iteration 1 to Iteration 2, the $k_{1,0}$ values typically changed by only ~2% (i.e., within the fitting uncertainty of the $k_{1,0}$ determination; see the next paragraph) and E_a changed by only 15 cal/mol. Therefore, only two iterations were performed. See Table S1 for more details.

Figure 4 displays a detailed $k_{1,0}$ uncertainty analysis of the Fig. 1 experiments. Six uncertainty sources $(k_{1,\infty}, k_2, k_3, T_5, \text{ mixture})$ composition, and fitting) were investigated by varying each source according to its estimated uncertainty and assessing the resultant change in $k_{1,0}$. The dominant uncertainty source is T_5 , followed by k_2 and k_3 . The visually estimated fitting uncertainty depends on the SNR and the sensitivity to R1. The uncertainty in $k_{1,\infty}$ has no discernible effect on $k_{1,0}$ because the conditions of the present study $(5.3 \times 10^{-6} \le [M] \le 1.1 \times 10^{-5} \text{ mol/cm}^3, 2476 \ge T_5 \ge 1546 \text{ K})$ are well within the low-pressure limit of R1. (Using $k_{1,\infty}$ from [15], [M]_{1/2} was estimated at 7.0 \times 10⁻⁴ and 5.0 \times 10⁻⁴ mol/cm³ at the high- and low-temperature ends of this study, respectively. As further evidence that the present conditions were within the low-pressure limit, using a $k_{1,\infty}$ expression with a broader Troe falloff curve [41] instead of a narrower Lindemann curve caused no change in the extracted $k_{1,0}$ values). The uncertainty in mixture composition has no discernible effect on $k_{1,0}$ largely due to the self-calibrating feature of these experiments; this self-calibrating feature also eliminates uncertainty in $k_{1,0}$ from spectroscopic parameters or laser frequency. The slight (< 10%) errors in the $k_{\nu,0}$

Combustion and Flame xxx (xxxx) xxx

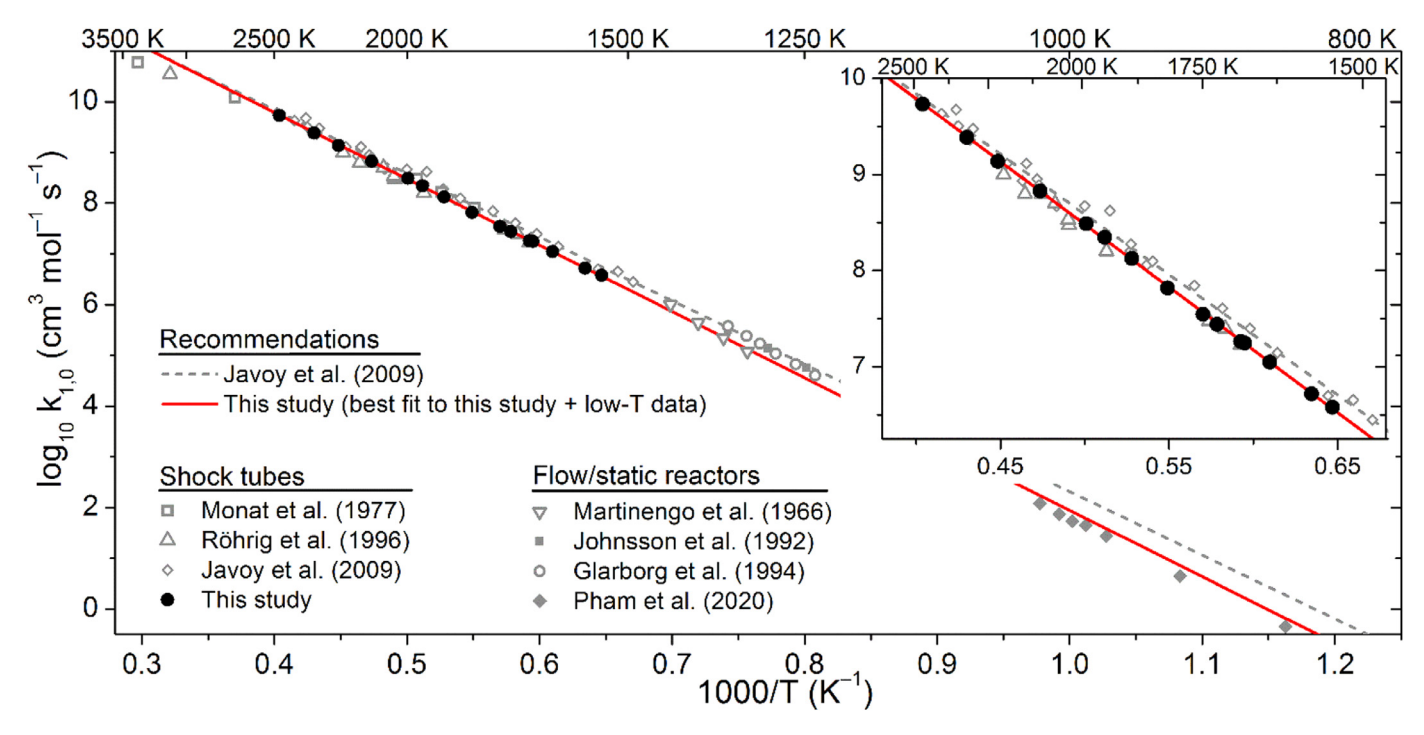


Fig. 5. Experimental $k_{1,0}$ values: the shock-tube studies of Monat et al. [4], Röhrig et al. [15], Javoy et al. [17] and this work and the flow/static reactor studies of Martinengo et al. [47], Johnsson et al. [48], Glarborg et al. [49], and Pham et al. [50]. The data from [48] shown here are the three datapoints that were reanalyzed in [49]. The recommendation by Javoy et al. was used in two recent chemical kinetics mechanisms [30,51]. The solid line is the combined fit to the data of this study and the low-temperature data. The Monat et al. data are not shown in the inset. The uncertainty bars of the present study are smaller than the symbols.

determination at high temperatures contribute only second-order errors to the second-order $k_{v,0}(T)$ correction to X_{N2O} (see Fig. S4); consequently, high-temperature uncertainty in $k_{v,0}$ has a negligible effect on both X_{N2O} and $k_{1,0}$. Combining the uncertainty sources using the root-sum-squares method yields total $k_{1,0}$ uncertainties of 8.9% and 9.0% for Fig. 1a and b, respectively. For the coldest experiment, the fitting uncertainty (~10%) dominates, leading to a total $k_{1,0}$ uncertainty of 13.0% at 1546 K.

The experimental $k_{1,0}$ values are plotted in Fig. 5. The best fit to the data of this study (1546–2476 K) is $k_{1,0}=1.01\times 10^{15}\exp(-59,715/RT)$ (units of cal, mol, cm, s, K). The present data fall well within the scatter of the previous shock-tube studies by Monat et al. [4], Röhrig et al. [15], and Javoy et al. [17]. Lest it appear we have handpicked these datasets, Fig. S1 shows that the $k_{1,0}$ data of the present study bisect the aggregate data of Table 1. By combining the results of this study with previous studies [47–50] at lower temperatures (860–1431 K), a best fit from 850 to 2500 K is obtained as $k_{1,0}=(1.04\pm0.04\times10^{15})\exp[(-59,810\pm180)/RT]$ (units of cal, mol, cm, s, K).

4. Discussion

4.1. Sensitivity to k_2 and k_3

Uncertainties in k_2 and k_3 each introduce 3–4% uncertainty in $k_{1,0}(\text{Fig. 4})$. Interestingly, a fair amount of controversy surrounds k_2 , particularly at lower temperatures (~950–1100 K). It was long accepted that $k_2 \approx k_3$ across a wide temperature range (see [34]). Gradually, several studies began to question this assumption, culminating in the comprehensive review by Meagher and Anderson [34] that proposed k_2 and k_3 with significantly different E_a values: $k_2 = 3.69 \times 10^{12} \exp(-15, 937/RT)$ and $k_3 = 9.15 \times 10^{13} \exp(-27, 682/RT)$. However, the recent review by Glarborg et al. [49]has again suggested that $k_2 = k_3$. Very recently, the

studies of Pham et al. [50]and Zhou et al. [52] have provided new evidence that $k_2 \neq k_3$ at lower temperatures, lending support to the k_2 expression of Meagher and Anderson. Note that k_2 is the controversial rate; k_3 seems to largely be agreed upon.

In light of the new experimental evidence [50,52], the Meagher and Anderson k_2 and k_3 seem the most trustworthy, so these values were adopted in the 26-reaction mechanism of the present study. Regardless of the final consensus on k_2 at lower temperatures, however, there seems to be little controversy regarding k_2 at higher temperatures: various sources agree $k_2 \approx k_3$ between 1800 and 2000 K [34,51]. Therefore, the 50% estimates of uncertainty in k_2 and k_3 [41] used in Fig. 4 should encompass the uncertainty introduced to $k_{1,0}$ by k_2 and k_3 in the present study (1546–2476 K). Future updates to k_2 and/or k_3 may require slight changes to our $k_{1,0}$ values.

4.2. Shock-tube modeling considerations

Modeling dP/dt using the VTIM method during the determination of $k_{1,0}$ had significant effects on the extracted $k_{1,0}$. As an example, consider the experiment shown in Fig. 6. The experimental pressure trace (Fig. 6a) displays an initial decrease followed by a gradual increase. The initial decrease in pressure (i.e., negative dP/dt) is a result of the relatively low pressures (1.1–1.4 atm) employed in this study and has been shown recently to be due to the transition of the boundary layer from laminar to turbulent [53](this negative dP/dt precludes the use of driver inserts [54], which can only correct for positive dP/dt). Also shown in Fig. 6a is a smoothed fit to the experimental pressure, P(t). From P(t), a normalized V(t) was calculated assuming isentropic expansion/compression (Fig. 6b). $V(t)/V_0$ deviates by almost 3% from the constant-V assumption, resulting in an isentropic temperature decrease of 29 K. Figure 6c shows the predictions of the 26reaction mechanism for two cases: one with constant V and one with the calculated V(t). The discrepancy between the constant-V

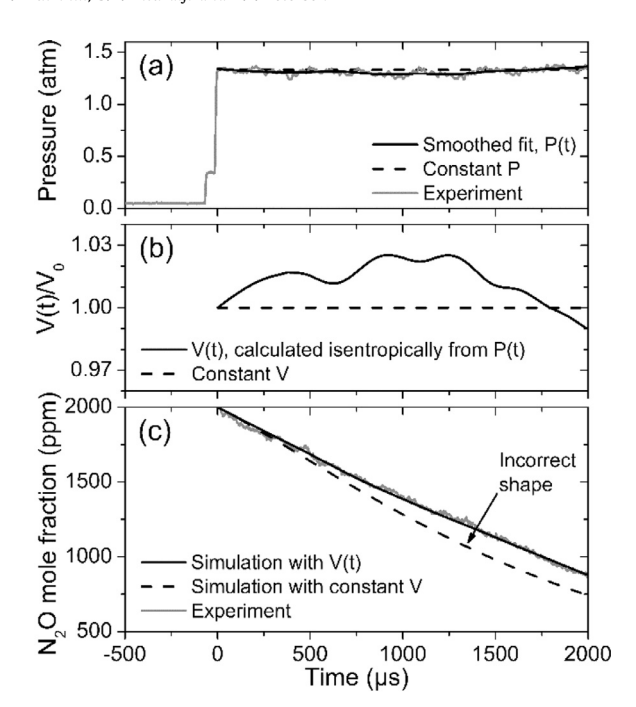


Fig. 6. Effect of dP/dt on the $k_{1.0}$ extraction for an experiment at 1754 K, 1.33 atm in 0.2% N₂O, balance Ar. (a) Experimental pressure time history and smoothed fit, P(t). (b) Normalized V(t) calculated isentropically from P(t). (c) Simulated N₂O time histories using the 26-reaction mechanism incorporating either constant V or V(t); the experimental time history is also shown. The dashed lines represent the constant-pressure behavior of an ideal shock tube.

and V(t) modeling cases in Fig. 6c translates to a 15% change in the extracted $k_{1.0}$ as well as poorer agreement with the experiment in terms of profile shape. Although the VTIM method was used to analyze all experimental data, the effects illustrated in Fig. 6c were strongest at lower temperatures: at higher temperatures ($T_5 > 1900 \text{ K}$), the N₂O decomposition occurs rapidly enough that dP/dt has little effect on the extracted $k_{1.0}$,

Proper modeling of dP/dt effects via V(t) is contingent upon a temperature-dependent Arrhenius expression. One method for extracting rate constants from speciation data is to fit mechanism predictions to data through varying k by changing A with E_a set equal to 0. Such methodology is straightforward, but removes the temperature dependence of the rate constant and negates the benefit of the VTIM method: a mechanism with $E_a=0$ for $k_{1,0}$ produces essentially identical results to the dashed line in Fig. 6c even if the modeling includes V(t). (Additionally, using $E_a=0$ largely negates the benefit of chemical kinetics solvers that account for temperature changes due to reactivity.) The $k_{1,0}$ iteration method described in Section 3 was employed to avoid the pitfalls of using $E_a=0$.

To facilitate accurate modeling of our experimental results by future researchers, the full experimental datasets for all 15 experiments, including the pressure traces, are provided in the SM.

4.3. Previous shock-tube studies of $k_{1,0}$

The $k_{1,0}$ data of this study represent the highest-precision shock-tube measurement of $k_{1,0}$ to date. This fact is quantified by the σ column in Table 1, which was calculated for each study by collecting all $k_{1,0}$ datapoints and taking the percent difference between each datapoint and the best-fit Arrhenius curve to the data; the standard deviation of the resulting distribution is σ . The σ value of the present study (3.1%) is almost three times smaller than the next smallest σ value and over ten times smaller than the largest σ values.

The hottest two datapoints in Fig. 5, from Monat et al. [4] and Röhrig et al. [15], are the hottest datapoints among all the Table 1 studies and fall ~50% below the best fit of this study. Simulations of the Monat et al. datapoint (2% N₂O in balance Ar, 3423 K, 0.37 atm) using the 26-reaction mechanism indicate that 50% of the N₂O decomposes after only ~3 µs. However, the obfuscation of the emission signal by the RSW in the sample trace in their Fig. 1 at 2500 K persists for ~4 µs, which would encompass most of the useful experimental time at 3423 K. Furthermore, their stated time resolution was 2 µs. Therefore, although Monat et al. and Röhrig et al. accounted for the RSW obfuscation issue via an exponential extrapolation, it is likely that their hottest experiments were still hindered by issues of time resolution and RSW obfuscation. To check for similar issues in the hottest experiment of the present study (2476 K), it was assumed that 10% of the initial N_2O decomposed during the passage of the RSW (based on the temporal width of the schlieren spike in the laser transmission signal during the RSW passage, ~7 μ s) such that X_{N2O} immediately behind the RSW was 0.18%. A kinetic analysis revealed no change in the bestfit $k_{1,0}$ despite this assumption, indicating the present experiments avoided RSW obfuscation issues.

Combustion and Flame xxx (xxxx) xxx

4.4. Previous low-temperature studies of $k_{1.0}$

The best-fit $k_{1,0}$ of the present study was slightly adjusted to compromise between four low-temperature studies: the flow reactor studies of Martinengo et al. [47], Johnsson et al. [48], and Glarborg et al. [49] and the static reactor study of Pham et al. [50]. The data of Johnsson et al. and Glarborg et al. are 40–80% higher than the present study, while the data of Pham et al. are 30–35% lower than the present study (Fig. 5).

The data of Glarborg et al. [49] possess a relatively steep slope $(E_a \approx 68,000 \text{ cal/mol})$. We contacted Dr. Peter Glarborg regarding this observation. He suggested this was due to N₂O decomposing in the preheat region of the flow reactor, which would lead to erroneously high values of $k_{1,0}$ and E_a . He also shared that this possibility did not occur to the authors of [49]at the time since their flow reactor was designed for hydrocarbon/oxidizer mixtures (the preheat zone problem is now well known to the flow reactor community; see Dryer et al. [55]). We modeled the flow reactor used in [49] with the assumption of a 2-6 cm preheat region before the reaction zone and an initial preheat inlet flow of 0.75% N₂O in balance Ar; these assumptions were based on descriptions of the experimental apparatus and discussions with Dr. Glarborg. The conclusion of these calculations is that when the preheat zone is considered, the $k_{1,0}$ data of [49] shift significantly downward and can thus be reconciled with the best-fit $k_{1,0}$ of this study; see the SM. A similar correction could be applied to the Johnsson et al. data [48], which are from the same facility.

Pham et al. [50] measured N_2O time histories in a static reactor between 860 and 1023 K at 1.05 atm. In modeling their N_2O time histories, they did not consider that their experimental conditions were somewhat in the falloff region. Assuming a Lindemann curve with $k_{1,\infty}$ from Röhrig et al. [15] and $k_{1,0}$ from our study, consideration of falloff behavior would increase the Pham et al. $k_{1,0}$ data by 4–6% (i.e., closer to our best-fit $k_{1,0}$). A broader, more accurate falloff curve would shift their data even closer to our best-fit $k_{1,0}$. (As an aside, the experimental data of Pham et al. were taken from the thesis by Tsay [56]. However, in their Fig. 1b, Pham et al. incorrectly copied the N_2O time histories from Tsay's Fig. 2.4. The correct data are given in Fig. S6).

Table 2 summarizes the recent $k_{1,0}$ expressions for M = Ar. The best fit of the present study combined with the low-temperature data is in excellent agreement with the recent values of E_a . Relative to the $k_{1,0}$ of the present study, the experimentally derived $k_{1,0}$ from Javoy et al. (which was recently used in two influential

JID: CNF

Combustion and Flame xxx (xxxx) xxx

Table 2 Arrhenius expressions for $k_{1,0}$ with M = Ar from recent studies.

Author	Year	Method	T range (K)	A ^a	nª	E_a^{a}	Ref.
Baulch et al.	2005	Review	1000-3000	6.02×10^{14}	0	57,450	[41]
Javoy et al.	2009	Experiment	1500-2500	7.20×10^{14}	0	57,386	[17]
Pham et al.	2020	Theory and experiment	850-1025 b	9.33×10^{14}	0	60,150	[50]
This study	2020	Experiment	1550-2500	1.01×10^{15}	0	59,715	-
This study $+$ low-T data	2020	Experiment and review	850-2500	1.04×10^{15}	0	59,810	-

^a Arrhenius expressions given as $k_{1,0} = AT^n \exp(-E_a/RT)$. Units are cal, mol, cm, s, K.

chemical kinetics mechanisms [30,51]) is 27% larger at 2000 K and a factor of 2.3 larger at 1000 K, while the theoretically calculated $k_{1,0}$ from Pham et al. [50] is 31% smaller at 1000 K and 25% smaller at 2000 K.

A three-parameter Arrhenius expression was also determined and is given by $k_{1.0}=1.70\times 10^{15}~T^{0.29}\exp(-60,800/RT)$ (units of cal, mol, cm, s, K). This expression deviates from the two-parameter fit by no more than 4.6% between 850 and 2500 K and may be employed as an alternative fit in this temperature range.

5. Conclusions

A new, fixed-wavelength laser absorption diagnostic near 4.56 µm was employed to measure N₂O time histories in shockheated mixtures of 0.2% N₂O in balance Ar between 1546 and 2476 K near 1.3 atm. Through a detailed chemical kinetic analysis including consideration of dP/dt effects, the low-pressure limit rate constant $k_{1,0}$ was extracted from the experimental data. By combining the new data with previous low-temperature data, a best fit was determined to be $k_{1,0} = (1.04 \pm 0.04 \times 10^{15}) \exp[(-30,098 \pm 0.04 \times 10^{15})]$ 90)/T] ($k_{1.0}$ in cm³mol⁻¹s⁻¹, T in K). Estimated uncertainties at 1546, 1821, and 2230 K are 13.0%, 8.9%, and 9.0%, respectively. The new $k_{1,0}$ data exhibit noticeably less scatter than all previous shock-tube studies and bisect the preponderance of the historical shock-tube data on $k_{1,0}$. Through careful experimental design, diagnostic deployment, and data analysis, the present study using N2O-IRA avoids the issues experienced by previous $k_{1,0}$ studies that employed N₂O-UVA, N₂O-IRE, and O-ARAS.

All experimental data from this study are provided in the SM. This transparency will aid future researchers in properly utilizing the high-quality data of this study via modeling of dP/dt behavior.

The present study seems particularly apt for this special issue honoring Ron Hanson since the thrust of the present work (accurate extraction of a rate constant from high-SNR laser absorption data via consideration of non-ideal shock-tube effects) is an extension of many methodologies promulgated by the Hanson Group over several decades. Shock-tube physics, laser diagnostics, atomic/molecular spectroscopy, and chemical kinetics have each benefitted immensely from Professor Hanson's illustrious career at Stanford University, and these fields will undoubtedly continue to bear his stamp for many years to come. As the field of combustion continues to grow and evolve, Ron's ongoing legacy will continue to inspire combustion researchers to reach new heights of understanding and achievement.

Declaration of Competing Interest

The authors declare that they have no known competing financial interests or personal relationships that could have appeared to influence the work reported in this paper.

Acknowledgments

The authors thank Dr. Peter Glarborg for open discussions regarding experimental facilities and for sharing the report describing his flow reactor. We also thank Dr. Francis M. Haas for helpful conversations about N_2O kinetics and for sharing his manuscript. Funding for this work was provided in part by the TEES Turbomachinery Laboratory and by the National Science Foundation, award number CBET-1706825. Additional fellowship funding support for the second author was provided from King Fahd University of Petroleum & Minerals (Fellowship No. 1440/10079/9) through the Saudi Arabian Cultural Mission.

Supplementary materials

Supplementary material associated with this article can be found, in the online version, at doi:10.1016/j.combustflame.2020.10.040.

References

- W. Jost, K.W. Michel, J. Troe, H.G. Wagner, Investigation of the thermal decomposition of N₂O in shock waves (translated title), Z. Naturforschung A 19 (1964) 59–64.
- [2] E. Stokes Fishburne, R. Edse, Shock-tube study of nitrous oxide decomposition, J. Chem. Phys. 41 (1964) 1297–1304.
- [3] H.A. Olschewski, J. Troe, H.G. Wagner, Low-pressure and high-pressure limits of N₂O decomposition (translated title), Ber. Bunsenges. Phys. Chem. 70 (1966) 450–459
- [4] J.P. Monat, R.K. Hanson, C.H. Kruger, Kinetics of nitrous oxide decomposition, Combust, Sci. Technol. 16 (1977) 21–28.
- [5] P. Roth, T. Just, Atomic absorption measurements for the kinetics of the reaction CH₄+O→CH₃+OH in the temperature range 1500<T<2250K (translated title), Ber. Bunsenges. Phys. Chem. 81 (1977) 572.</p>
- [6] S.C. Barton, J.E. Dove, Mass spectrometric studies of chemical reactions in shock waves: The thermal decomposition of nitrous oxide, Can. J. Chem. 47 (1969) 521–538.
- [7] W.H. Lipkea, D. Milks, R.A. Matula, Nitrous oxide decomposition and its reaction with atomic oxygen, Combust. Sci. Technol. 6 (1973) 257–267.
- [8] J.E. Dove, W.S. Nip, H. Teitelbaum, The vibrational relaxation and pyrolysis of shock heated nitrous oxide, Symp. (Int.) Combust., 15 (1975), pp. 903–916.
- [9] I.S. Zaslonko, A.S. Losev, E.V. Mozzhukkin, Y.K. Mukoseev, Thermal decomposition of N₂O in Ar, He, N₂, or CO atmospheres, Kin. Catal. 21 (1980) 311–315 (Translated from Kinetica i Kataliz).
- [10] K.G.P. Sulzmann, J.M. Kline, S.S. Penner, Shock-tube studies of N₂O-decomposition, 12th International Symposium on Shock Tubes and Waves, 1980.
- [11] N. Fujii, S. Uchida, H. Sato, S. Fujimoto, H. Miyama, High-temperature reaction of NH₃-N₂O system in shock waves, Bull. Chem. Soc. Jpn. 59 (1986) 3431–3437.
- [12] N. Fujii, S. Sagawai, T. Sato, Y. Nosaka, H. Miyama, Study of the thermal dissociation of nitrous oxide and carbon dioxide using oxygen(³P) atomic resonance absorption spectroscopy, J. Phys. Chem. 93 (1989) 5474–5478.
- [13] A.P. Zuev, A.Y. Starikovskii, Reactions involving nitrogen oxides at high temperatures. Monomolecular decay of $\rm N_2O$ (translated title), Khim. Fiz. 10 (1991) 52–63.
- [14] J.V. Michael, K.P. Lim, Rate constants for the N_2O reaction system: Thermal decomposition of N_2O ; $N+NO\rightarrow N_2+O$; and implications for $O+N_2\rightarrow NO+N$, J. Chem. Phys. 97 (1992) 3228–3234.
- [15] M. Röhrig, E.L. Petersen, D.F. Davidson, R.K. Hanson, The pressure dependence of the thermal decomposition of N₂O, Int. J. Chem. Kinet. 28 (1996) 599–608.

^b This T range corresponds to their experiments. They found good agreement between their theoretically calculated $k_{1,0}$ and both (1) their low-temperature data and (2) the high-temperature data of Monat et al. [4] (see Section 4.3 regarding the highest-temperature Monat et al. data).

- [16] S.K. Ross, J.W. Sutherland, S.-.C. Kuo, R.B. Klemm, Rate constants for the thermal dissociation of N_2O and the $O(^3P)+N_2O$ reaction, J. Phys. Chem. A 101 (1997) 1104–1116.
- [17] S. Javoy, R. Mevel, C.E. Paillard, A study of N₂O decomposition rate constant at high temperature: Application to the reduction of nitrous oxide by hydrogen, Int. J. Chem. Kinet. 41 (2009) 357–375.
- [18] R.K. Hanson, S. Salimian, Survey of rate constants in the N/H/O system, in: W.C. Gardiner (Ed.), Combustion Chemistry, Springer-Verlag, New York, NY (1984), pp. 361–421.
- [19] M.G. Holliday, B.G. Reuben, Temperature dependence of the absorption of nitrous oxide in the quartz ultra-violet, Trans. Faraday Soc. 64 (1968) 1735–1741.
- [20] A.P. Zuev, A.Y. Starikovskii, UV absorption cross section of the molecules O₂, NO, N₂O, CO₂, H₂O, and NO₂, J. App. Spectr. 52 (1990) 304–313.
- [21] C.E. Moore, Selected Tables of Atomic Spectra, Atomic Energy Levels and Multiplet Tables, National Bureau of Standards (1976), p. 7. National Standard Reference Data Series 3, Sec. 7.
- [22] A. Shastri, P.J. Singh, S. Krishnakumar, A. Mandal, B.N. Raja Sekhar, R. D'Souza, B.N. Jagatap, Vibronic and Rydberg series assignments in the vacuum ultraviolet absorption spectrum of nitrous oxide, J. Quant. Spec. Rad. Trans. 147 (2014) 121–133
- [23] G.A. Pang, D.F. Davidson, R.K. Hanson, Experimental study and modeling of shock tube ignition delay times for hydrogen-oxygen-argon mixtures at low temperatures, Proc. Combust. Inst. 32 (2009) 181–188.
- [24] M. Razeghi, W. Zhou, S. Slivken, Q.--Y. Lu, D. Wu, R. McClintock, Recent progress of quantum cascade laser research from 3 to 12 μm at the center for quantum devices, Appl. Opt. 56 (2017) H30–H44.
- [25] C.S. Goldenstein, R.M. Spearrin, J.B. Jeffries, R.K. Hanson, Infrared laser-ab-sorption sensing for combustion gases, Prog. Energy Combust. Sci. 60 (2017) 132–176.
- [26] R.K. Hanson, Applications of quantitative laser sensors to kinetics, propulsion and practical energy systems, Proc. Combust. Inst. 33 (2011) 1–40.
- [27] E.L. Petersen, A Shock Tube and Diagnostics for Chemistry Measurements at Elevated Pressures With Application to Methane Ignition, Ph.D. dissertation, Stanford University, 1998.
- [28] E.L. Petersen, R.K. Hanson, Nonideal effects behind reflected shock waves in a high-pressure shock tube, Shock Waves 10 (2001) 405–420.
- [29] J.E. Vivanco, A New Shock-Tube Facility for the Study of High-Temperature Chemical Kinetics, M.S. thesis, Texas A&M University, 2014.
- [30] Y. Zhang, O. Mathieu, E.L. Petersen, G. Bourque, H.J. Curran, Assessing the predictions of a NOx kinetic mechanism on recent hydrogen and syngas experimental data, Combust. Flame 182 (2017) 122–141.
- [31] J. Urzay, N. Kseib, D.F. Davidson, G. Iaccarino, R.K. Hanson, Uncertainty-quantification analysis of the effects of residual impurities on hydrogen-oxygen ignition in shock tubes, Combust. Flame 161 (2014) 1-15.
- [32] C.R. Mulvihill, S.A. Alturaifi, O. Mathieu, E.L. Petersen, A N₂O Laser Absorption Diagnostic Near 4.6 μm for Shock-Tube Chemical Kinetics Studies, AIAA SciTech Forum, 2020.
- [33] L.S. Rothman, I.E. Gordon, R.J. Barber, H. Dothe, R.R. Gamache, A. Goldman, V.I. Perevalov, S.A. Tashkun, J. Tennyson, HITEMP, the high-temperature molecular spectroscopic database, J. Quant. Spec. Rad. Trans. 111 (2010) 2139–2150.
- [34] N.E. Meagher, W.R. Anderson, Kinetics of the $O(^3P)+N_2O$ reaction. 2. Interpretation and recommended rate coefficients, J. Phys. Chem. A 104 (2000) 6013–6031.
- [35] A.M. Mebel, M.C. Lin, K. Morokuma, C.F. Melius, Theoretical study of reactions of N₂O with NO and OH radicals, Int. J. Chem. Kinet. 28 (1996) 693–703.
- [36] W. Tsang, J.T. Herron, Chemical kinetic data base for propellant combustion I. Reactions involving NO, NO₂, HNO, HNO₂, HCN and N₂O, J. Phys. Chem. Ref. Data 20 (1991) 609–663.

- [37] M. Abian, M.U. Alzueta, P. Glarborg, Formation of NO from N₂/O₂ mixtures in a flow reactor: Toward an accurate prediction of thermal NO, Int. J. Chem. Kinet. 47 (2015) 518–532.
- [38] J. Park, N.D. Giles, J. Moore, M.C. Lin, A comprehensive kinetic study of thermal reduction of NO₂ by H₂, J. Phys. Chem. A 102 (1998) 10099–10105.
- [39] J. Hahn, K. Luther, J. Troe, Experimental and theoretical study of the temperature and pressure dependences of the recombination reactions O+NO₂(+M)→NO₃(+M) and NO₂+NO₃(+M)→N₂O₅(+M), Phys. Chem. Chem. Phys. 2 (2000) 5098–5104.
- [40] W. Tsang, R.F. Hampson, Chemical kinetic data base for combustion chemistry. Part I. Methane and related compounds, J. Phys. Chem. Ref. Data 15 (1986) 1087–1279.
- [41] D.L. Baulch, C.T. Bowman, C.J. Cobos, R.A. Cox, T. Just, J.A. Kerr, M.J. Pilling, D. Stocker, J. Troe, W. Tsang, R.W. Walker, J. Warnatz, Evaluated kinetic data for combustion modeling: Supplement II, J. Phys. Chem. Ref. Data 34 (2005) 757–1397.
- [42] A. Burcat, B. Ruscic, Third Millenium Ideal Gas and Condensed Phase Thermochemical Database for Combustion, Argonne National Laboratory and Technion-Israel Institute of Technology, Chicago, IL, 2005, Report No. ANL-05/20 and TAE 960.
- [43] G. Rudinger, Effect of boundary-layer growth in a shock tube on shock reflection from a closed end, Phys. Fluids 4 (1961) 1463–1473.
- [44] A. Farooq, J.B. Jeffries, R.K. Hanson, Sensitive detection of temperature behind reflected shock waves using wavelength modulation spectroscopy of CO₂ near 2.7 µm, Appl. Phys. B 96 (2009) 161–173.
- [45] M. Chaos, F.L. Dryer, Chemical-kinetic modeling of ignition delay: Considerations in interpreting shock tube data, Int. J. Chem. Kinet. 42 (2010) 143–150.
- [46] E.L. Petersen, M.J. Rickard, M.W. Crofton, E.D. Abbey, M.J. Traum, D.M. Kalitan, A facility for gas- and condensed-phase measurements behind shock waves, Meas. Sci. Technol. 16 (2005) 1716–1729.
- [47] A. Martinengo, J. Troe, H.G. Wagner, Investigation of decomposition reactions with the method of adiabatic compression (translated title), Z. Phys. Chem. 51 (1966) 104–107.
- [48] J.E. Johnsson, P. Glarborg, K. Dam-Johansen, Thermal dissociation of nitrous oxide at medium temperatures, Symp. (Int.) Combust., 24 (1992), pp. 917–923.
- [49] P. Glarborg, J.E. Johnsson, K. Dam-Johansen, Kinetics of homogeneous nitrous oxide decomposition, Combust. Flame 99 (1994) 523–532.
- [50] T.V. Pham, T.J. Tsay, M.C. Lin, Thermal decomposition of N₂O near 900K studied by FTIR spectrometry: Comparison of experimental and theoretical O(³P) formation kinetics, Int. J. Chem. Kinet. 52 (2020) 632–644.
- [51] P. Glarborg, J.A. Miller, B. Ruscic, S.J. Klippenstein, Modeling nitrogen chemistry in combustion, Prog. Energy Combust. Sci. 67 (2018) 31–68.
- [52] M. Zhou, M.C. Barbet, R.E. Cornell, M.P. Burke, F.M. Haas, Intermediate temperature experiments constrain branching ratio of N₂O+O→products, Int. J. Chem. Kinet. (2020) J.V. Michael Special Issue. Submitted.
- [53] J.T. Lipkowicz, D. Nativel, S. Cooper, I. Wlokas, M. Fikri, E.L. Petersen, C. Schulz, A.M. Kempf, Numerical investigation of remote ignition in shock tubes, Flow Turb. Combust. (2020) in press, doi:10.1007/s10494-020-00219-w.
- [54] Z.K. Hong, G.A. Pang, S.S. Vasu, D.F. Davidson, R.K. Hanson, The use of driver inserts to reduce non-ideal pressure variations behind reflected shock waves, Shock Waves 19 (2009) 113–123.
- [55] F.L. Dryer, F.M. Haas, J. Santner, T.I. Farouk, M. Chaos, Interpreting chemical kinetics from complex reaction-advection-diffusion systems: Modeling of flow reactors and related experiments, Prog. Energy Combust. Sci. 44 (2014) 19–39.
- [56] T.J. Tsay, Application of Fourier Transform Infrared Spectrometry to Studies of Gas-Phase Kinetics: Thermal Decomposition Reactions of Nitrous Oxide and Diketene, M.S. thesis, Emory University, 1991.